(Received 24 November 2023, Accepted 28 December 2023, Scheduled 12 January 2024)

Antenna Sensor Based on an Inter-Digital Capacitor Shape EBG Structure for Liquid Dielectric Measurement

Bo Yin and Juntao Yin*

School of Optoelectronic Engineering, Chongqing University of Posts and Telecommunications, Chongqing 400065, China

ABSTRACT: In this paper, an antenna sensor based on an electromagnetic bandgap (EBG) structure is proposed to measure the complex permittivity of liquid under test (LUT). The sensor consists of two parts: a detection antenna and an EBG structure. The detection antenna uses a semicircular arc defective ground structure to improve the quality factor (Q-factor). Simultaneously, the EBG structure can be equivalent to a narrow-band bandpass filter, so that the electromagnetic wave can only propagate in a very narrow frequency band. It can further improve the Q-factor of the antenna and realize the precise positioning of the resonance frequency point. The complex permittivity of the LUT can be extracted by measuring the resonant frequency shift and the amount of variation in the Q-factor of the antenna. The test results show that the sensor can detect dielectric values covering the range of 1–25, and the average sensitivity is 2.342%. It combines the advantages of high sensitivity and wide detection range.

1. INTRODUCTION

The measurement of the relative complex permittivity, ε_r^* ($\varepsilon_r^* = \varepsilon_r - j\varepsilon_r'$), which describes the interaction between the material and electromagnetic field, has great potential for applications in food testing [1, 2], biomedicine [3–5], industrial chemistry [6–8], etc. It is mainly characterized by the real part: ε_r, which describes the energy stored in the material when it is passed by electromagnetic energy, and the loss tangent: $\tan\delta$ ($\tan\delta = \varepsilon_r'/\varepsilon_r$), which is related to the dissipation of energy in the material. In [9], Santra and Limaye proposed a dielectric sensor operating in the microwave band to measure the relative complex permittivity of materials. With strong robustness, real-time performance and label-free measurement compatibility, microwave sensors are highly adopted in various measurement and instrumentation applications.

To date, dielectric sensors operating in the microwave band can be categorized as resonant [10] and non-resonant [11]. Non-resonant methods utilize changes in the characteristic impedance and wave speed of electromagnetic waves to derive the dielectric constant of the material, such as free-space method [12], transmission line methods using waveguides [13], and coaxial wires [14]. The resonant method uses the principle of resonant perturbation to invert the dielectric constant from the change in resonant frequency and quality factor (Q-factor) [15]. Among these designs, resonant dielectric sensors are more advantageous due to their small size, high sensitivity, and low cost.

In 2020, Haq et al. proposed a two-port dielectric sensor based on complementary symmetric S-type resonant cavity (CSSSR) [16]. It utilizes the values of resonant frequency and depth of trapping to invert the dielectric constant of a solid material. Alam et al. proposed a dual-frequency sensor for detecting the dielectric constant of solid materials in 2022 [17]. The sensor structure consists of a pair of u-shaped resonators connected via a power divider and a microstrip feed line, thus generating two different sensing hotspots. It realizes simultaneous measurement of two samples at a time, dramatically improving the efficiency of testing.

Dielectric measurements of solid materials are relatively simple compared to liquid materials, since the dielectric loss of solid materials is usually much lower than that of liquids. When a high loss liquid under test (LUT) is loaded, the Q-factor of the overall system drops dramatically, making it difficult to determine the resonant frequency point [18]. This phenomenon greatly limits the range of application of sensors for liquid measurement. Therefore, liquid dielectric sensors require high intrinsic Q-factor to achieve test robustness in different environments. In conclusion, it is valuable to realize the accurate measurement of complex permittivity of LUTs with high loss tangent.

Liu and Tong presented a resonator based on the substrate-integrated waveguide (SIW) technology used as a complex dielectric constant measurement of aqueous ethanol in 2015 [19]. SIW technology utilizes metal vias on a dielectric substrate to realize the field propagation pattern of the waveguide, which dramatically improves the device's Q-factor. The disadvantage is that the sensor must be fully immersed in the LUT during measurement. Due to the corrosive and toxic nature of some liquids, the realization of non-contact measurement of LUTs is also a current research hotspot. In 2016, Seo et al. designed a sensor for ethanol concentration detection using one-eighth mode SIW (EMSIW) antenna and microfluidics [20]. It solves the problems of low Q-factor and contact measurements of conventional sensors. However, the maximum frequency shift is only 130 MHz when ethanol is loaded in the concen-

* Corresponding author: Juntao Yin (1241602805@qq.com).

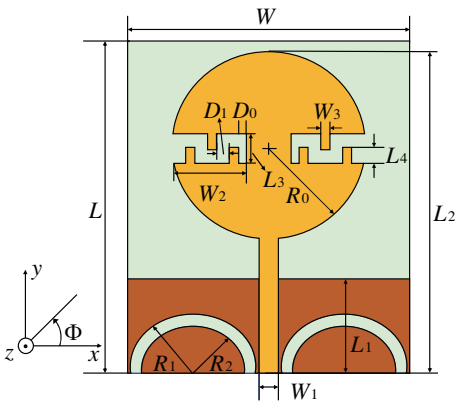

FIGURE 1. CPW monopole antenna configuration.

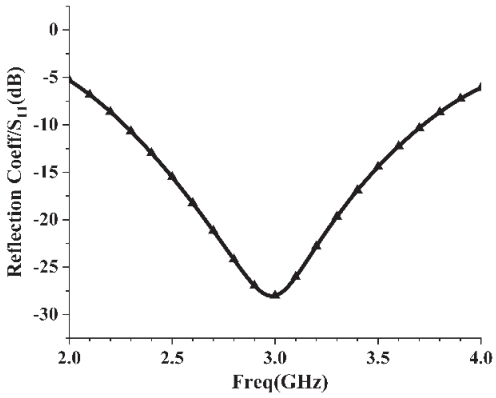

FIGURE 2. S_{11} parameter of single antenna.

TABLE 1. Parameters of the proposed antenna and EBG element.

Parameter	Value/mm	Parameter	Value/mm	Parameter	Value/mm
W	35	L_3	4	De_0	4
L	42	L_4	2	De_1	6
W_1	2.4	R_0	12.8	We_1	2
W_2	9.8	R_1	7.6	We_2	2
W_3	1	R_2	5.6	Le_1	38
L_1	12	D_0	1	G_1	6
L_2	40.8	D_1	2	G_2	6

tration range of 0–50%, and the detection sensitivity needs to be improved. In order to simultaneously satisfy the high sensitivity of the sensor and the non-contact measurement, Jun et al. presented a new method for liquid dielectric measurements [21], which uses a reconfigurable antenna in combination with a conventional rectangular patch-shaped electromagnetic bandgap (EBG) structure. The loading of the LUT causes a sharp change in the reflection phase of the EBG, which results in a highly sensitive frequency tuning of the detection antenna. Based on Jun et al.'s work, Arif et al. have improved the sensitivity of the sensor by etching special fractal grooves on the surface of the EBG element [22], which enhances the E-field strength in the sensing region by 19%. However, the complex topology of its EBG and antenna leads to the introduction of extraneous transmission zeros in the operating band interfering with the test, and the 3×3 EBG array also leads to a large overall size.

Based on the above work, this paper proposes an antenna sensor with a 2×2 EBG array, and the EBG array structure is similar to an inter-digital capacitor shape. The sensing channel of the LUT is placed on the EBG structure, which exists separately from the detection antenna. The detection antenna is not in contact with the LUT, which avoids corrosion of the detection antenna by the special LUT. The presence of the EBG array suppresses the surface waves radiated by the antenna and reduces the return loss of the antenna's radiated energy. The loading of the EBG improves the intrinsic Q-factor of the detection antenna and broadens the measurement range. Meanwhile, the EBG can pool a higher E-field strength in the sensing region, which increases the measurement sensitivity of the sensor. In this paper, the structural and geometrical parameters of the sensor components are firstly presented. Secondly, the introduction of sensing theory and simulation analysis of the antenna sensor loaded with EBG structure are given. Finally, the performance evaluation and validation of the measurement effect of the sensor is carried out. Compared with traditional dielectric sensors, this sensor has the advantages of non-contact measurement, high sensitivity, and wide measurement range.

2. ANTENNA SENSOR DESIGN AND CONFIGURATION

2.1. Design of Detection Antenna

The top view of the proposed antenna structure is shown in Figure 1. The overall size of the antenna is 35 mm $\times$ 42 mm $\times$ 1.6 mm. The proposed antenna is printed on a Teflon (F4B) substrate with a dielectric constant of 3.5, a loss tangent of 0.002, and a substrate thickness of 1.6 mm, Table 1 shows the specific structural parameters of the antenna. By designing the S-shaped open slot structure, the antenna surface equivalent current path is extended, and then the branch equivalent inductance value is adjusted to tune the resonant frequency. As shown in Figure 2, the antenna center frequency is located at 3 GHz and the -10 dB impedance bandwidth located in the 2.3–3.7 GHz frequency range. Part of the ground plane combined with the semi-arc etched groove helps to improve the impedance matching of

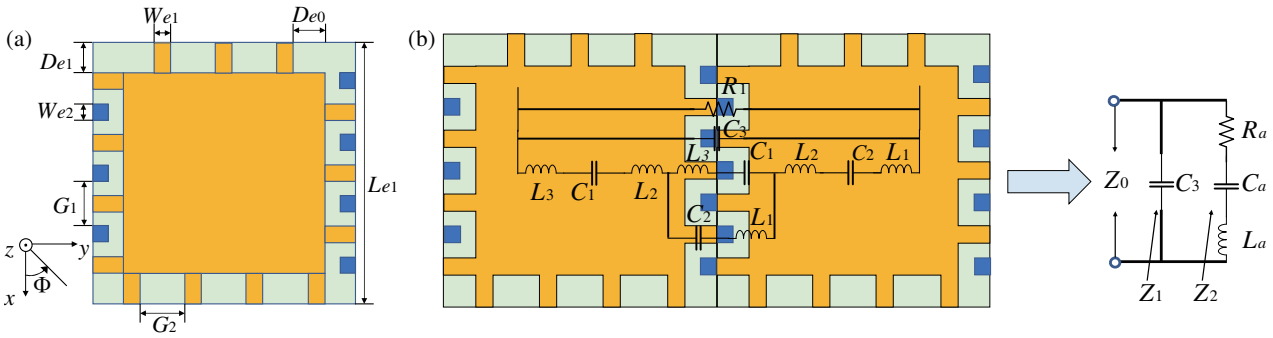

FIGURE 3. Geometry and equivalent circuit diagram of the EBG element structure. (a) Top view of the EBG element structure. (b) Equivalent circuit of the EBG element structure.

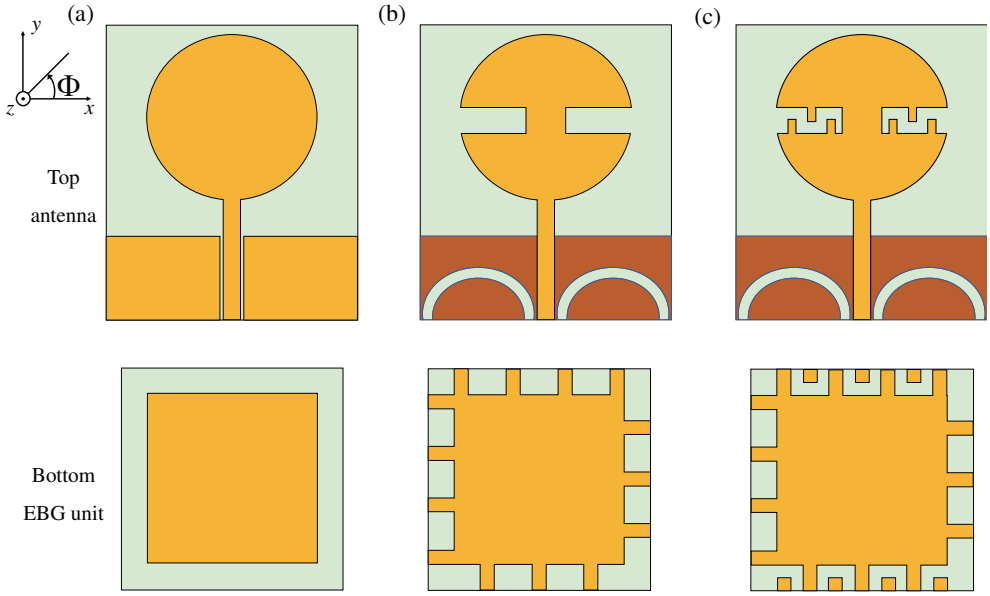

FIGURE 4. Evolution of the sensor. (a) Process 1. (b) Process 2. (c) Process 3.

the antenna, and the reflection coefficient at the resonance frequency point is below -25 dB.

2.2. Design of EBG Element

The EBG element topology used in this paper is shown in Figure 3(a). Due to the self-similar spatial distribution of the element structure, EBG elements arranged in a periodic structure will form an inter-digital capacitance structure at the horizontal gap between two elements, which will lead to a significant increase in the local electric field strength in this area, and placing the liquid to be measured in this area to measure its dielectric properties will significantly improve the test sensitivity of the sensor. The equivalent circuit of the elements is shown in Figure 3(b). The parasitic resistance R_a is frequency independent and can be neglected at high frequencies. A total equivalent input impedance and resonant frequency of the element can be obtained by the following equation.

$$Z_1 = -\frac{1}{j\omega C_3} \tag{1}$$

$$Z_2 \approx \frac{1-\omega^2 L_a C_a}{j\omega C_a} \tag{2}$$

$$Z_0 = \frac{Z_1 * Z_2}{Z_1 + Z_2} \approx \frac{1-\omega^2 L_a C_a}{j\omega(C_a + C_3 - \omega^2 L_a C_a C_3)} \tag{3}$$

$$f_r = \frac{1}{2\pi}\sqrt{\frac{C_a + C_3}{C_a L_a C_3}} \tag{4}$$

C_3 and C_a in the above equation represent the capacitance between the element patch and ground and the inter-digital capacitance between the two element patches, respectively, and L_a is the total equivalent parasitic inductance of the patch. From Equation (4), it can be seen that increasing the value of the capacitance and inductance helps to reduce the resonant frequency of the element to a lower frequency band.

3. THEORETICAL ANALYSIS

Floquet port excitation is used for the EBG element in High Frequency Structure Simulator (HFSS), which simulates the reflection phase of the periodic structure. With the addition of

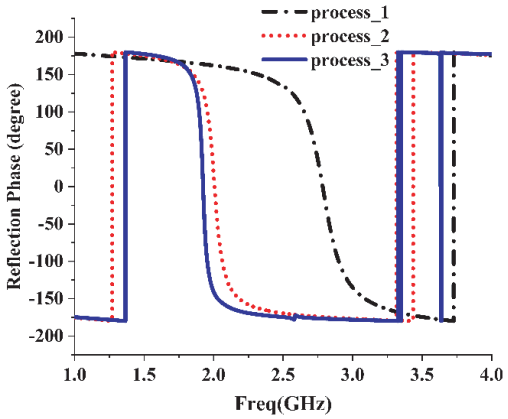

FIGURE 5. Simulated reflection phase of the EBG element.

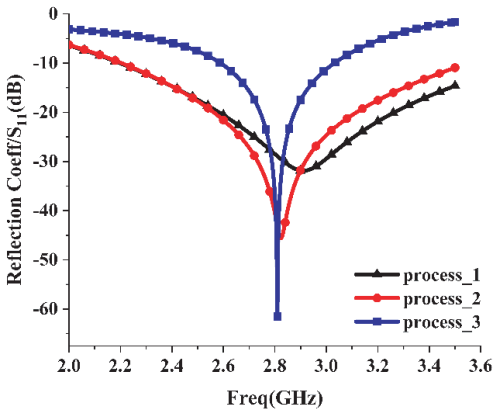

FIGURE 6. Simulated S_{11} of the three design processes.

patch branches, it will increase its equivalent inductance value and tune the 0 reflection phase point to a lower frequency position. Meanwhile, the trench formed by the EBG array will interrupt the surface wave propagation of the microstrip antenna, thus changing the reflected phase of the incident electromagnetic wave.

As shown in Figure 5, the $0 \pm 90°$ reflected phase interval of the EBG structure will be narrowed to cover $1.92 \sim 1.94$ GHz, and the frequency selection effect of the element will be more obvious, thus suppressing the influence of the surface wave of the antenna operating band on the radiation efficiency and reducing the subflap of the antenna radiation [23].

In order to determine the resonant frequency of the antenna and to avoid the resonance peak curve tends to show broadband characteristics when high permittivity and high loss tangent LUTs are loaded in the actual measurement. The sensor is required to have a high Q-factor characteristic, which is convenient to obtain the accurate resonant frequency from the S_{11} parameter map, thus improving the test resolution of the sensor. The Q-factor of the sensor can be derived from Equation (5), where f_r and BW represent the center resonant frequency and -3 dB frequency bandwidth, respectively.

$$Q = \frac{f_r}{BW} \tag{5}$$

Figure 4 illustrates the evolution of the sensor topology design, which was achieved through the iterative optimization of both the antenna and EBG element topology. By comparing the reflection coefficient curves of the three sensor structures, as shown in Figure 6, it is observed that the sensor gradually exhibits high Q characteristics. Furthermore, the S parameter plot in Figure 2 indicates that the resonance of the antenna becomes deeper, and the impedance bandwidth range is narrower when the EBG array structure is present, than a single antenna structure. These findings suggest that the antenna sensor loaded with an EBG structure of design process 3 possesses good impedance matching, which is supported by the S_{11} Smith chart diagram in Figure 8. Specifically, the equivalent input impedance of the sensor system tends towards 0 near the resonant frequency point of 2.8 GHz. Adequate impedance matching can effectively reduce the dissipation of transmission energy, which is conducive to maintaining the high Q-factor characteristics of the device.

The selected sensor architecture, as shown in Figure 7, employs F4B substrate material for both the detection antenna and EBG reflector. The substrate thickness is 2 mm for the reflector and 1.6 mm for the antenna. A PVC tube with a relative permittivity of 2.2 is used to load the LUTs, with an inner diameter of 2 mm and an outer diameter of 3 mm. Based on Equations (6) and (7), placing the LUT in the EBG array's area of maximum electric field strength can increase the sensor's frequency shift, thereby achieving higher test sensitivity. Here, f_r and f_0 represent the resonant frequencies of the loaded and unloaded LUTs, respectively.

Based on the electric field distribution presented in Figure 9, it can be observed that the antenna sensor loaded with an interdigital EBG structure exhibits a higher electric field strength at the slot area than the conventional rectangular patch EBG structure. This indicates that the overall system's Q-factor and sensitivity would be significantly improved. The radiation patterns of a monopole antenna and those of an EBG array-loaded antenna in Process 3 structure were compared. The results depicted in Figure 10 show that a single antenna has a bidirectional radiation pattern in all planes. In contrast, the radiation pattern of the antenna loaded with a planar EBG structure is more directional, with an approximately 10 dB improvement in the front-to-back ratio of the radiation pattern.

$$\frac{\Delta f}{f_0} \approx -\frac{\iiint_v \left(\Delta\mu \left|H_0\right|^2 + \Delta\varepsilon \left|E_0\right|^2\right) dv}{\iiint_v \left(\mu \left|H_0\right|^2 + \varepsilon \left|E_0\right|^2\right) dv} \tag{6}$$

$$S = \frac{\Delta f / f_r}{\Delta\varepsilon} = \frac{1}{N} \sum_{i=1}^{N} \frac{f_0 - f_r}{f_0(\varepsilon_r - \varepsilon_0)} \tag{7}$$

For the calculation of the complex permittivity of LUT, one of the best methods is to derive a mathematical model using a curve-fitting technique that generates an imperative equation that best fits a given set of data points. As shown in Figure 11, the S_{11} transmission response curves of the antenna when it is

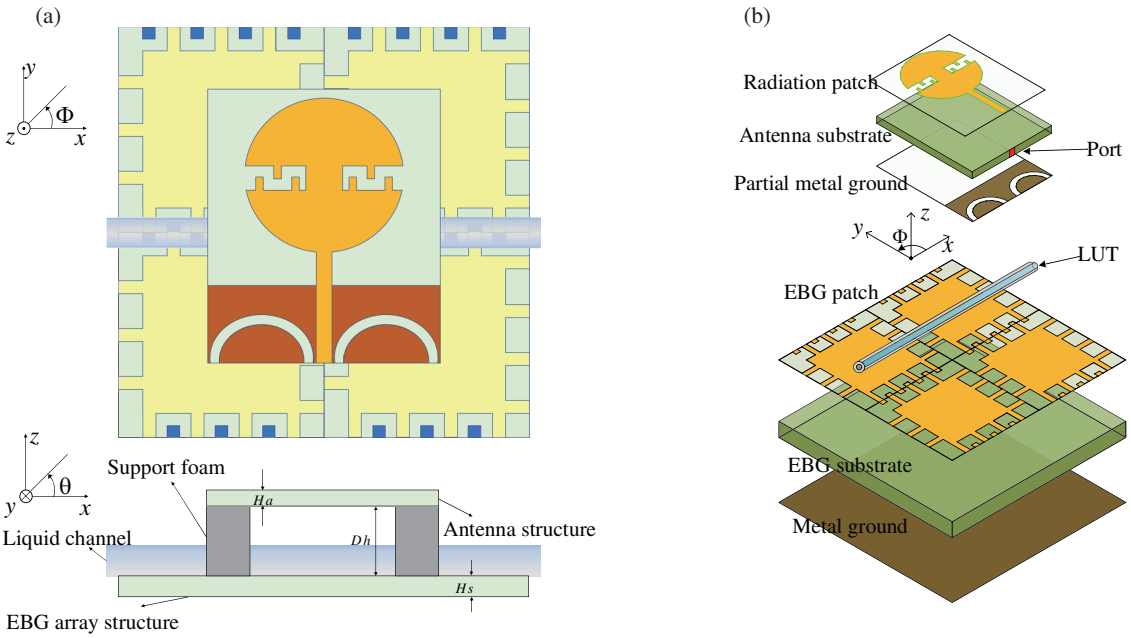

FIGURE 7. The final proposed sensor topology with liquid channel. (a) Top view and side view. (b) Exploded view.

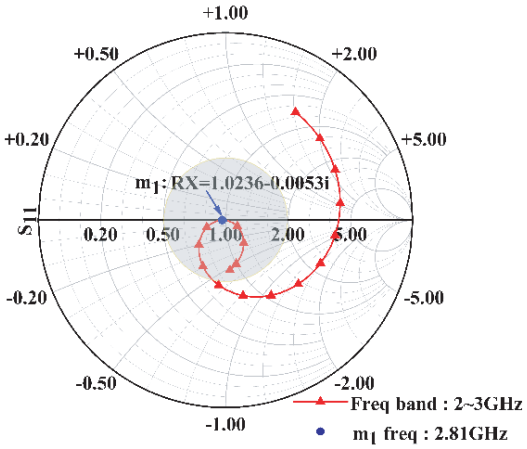

FIGURE 8. Simulated S_{11} smith chart of the final proposed antenna sensor.

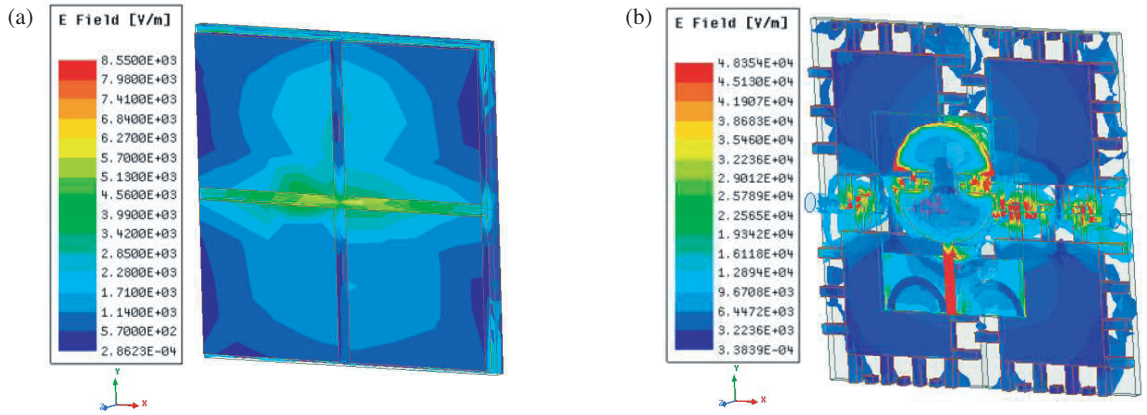

FIGURE 9. E-field profile of the 2 × 2 initial and modified EBG planes. (a) Simple square patch EBG plane. (b) Modified EBG plane.

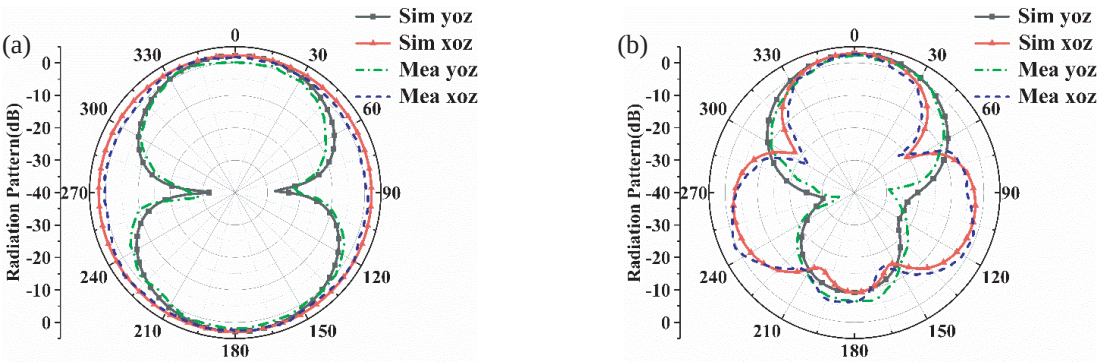

FIGURE 10. Radiation pattern of the proposed antenna sensor system at 2.8 GHz. (a) Sensor without EBG. (b) Sensor with EBG.

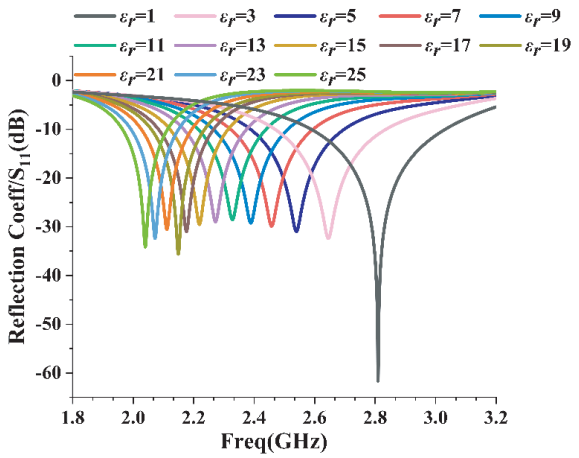

FIGURE 11. Simulated S_{11} of the antenna sensor with different relative permittivity of the liquid.

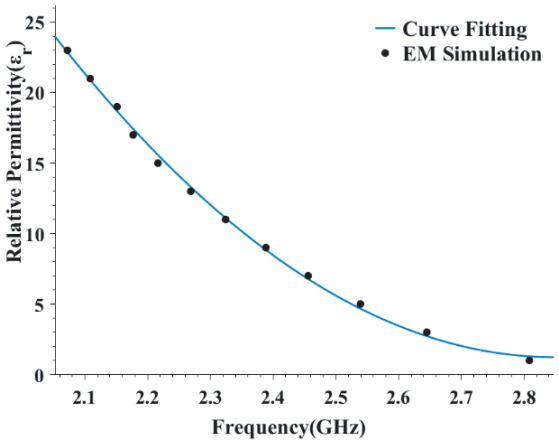

FIGURE 12. Relative permittivity (ε_r) of the LUT as a function of the normalized resonance frequency.

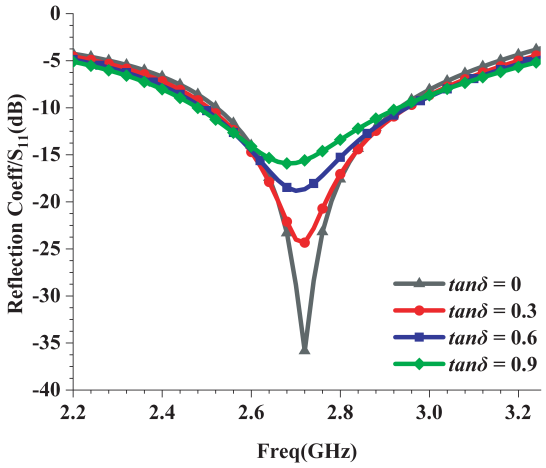

FIGURE 13. Simulated dependence of S_{11} on different loss tangents in the case of LUT $\varepsilon_r = 2$.

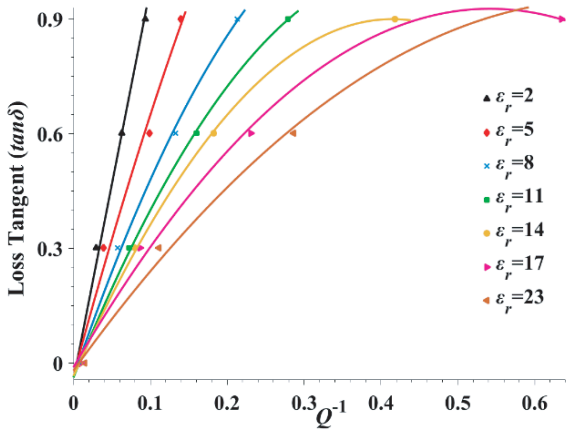

FIGURE 14. The loss tangent ($\tan\delta$) against the inverse normalized Q-factor for different value of ε_r.

loaded with LUTs of different relative permittivities were simulated using HFSS, and good resonant frequency shifts and S_{11} less than -10 dB were observed over a wide range of relative permittivity ($\varepsilon_r = 1$–25), implying that the sensor always has a good impedance match.

As shown in Figure 12, the scattered data of resonant frequency and the corresponding real part of the relative permittivity when loading different LUTs were fitted with MATLAB. The fitted curves of resonant frequency and relative permittiv-

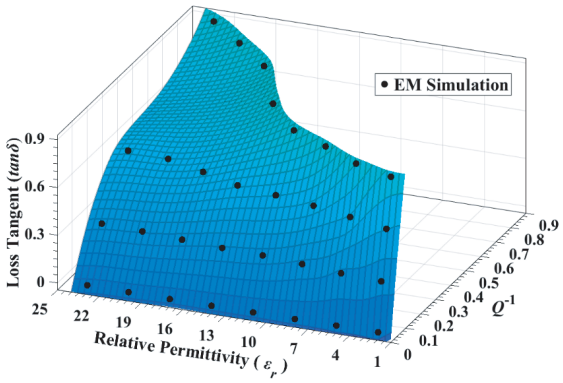

FIGURE 15. Trend diagram of the loss tangent ($\tan\delta$) corresponding to different values of ε_r and Q^{-1}.

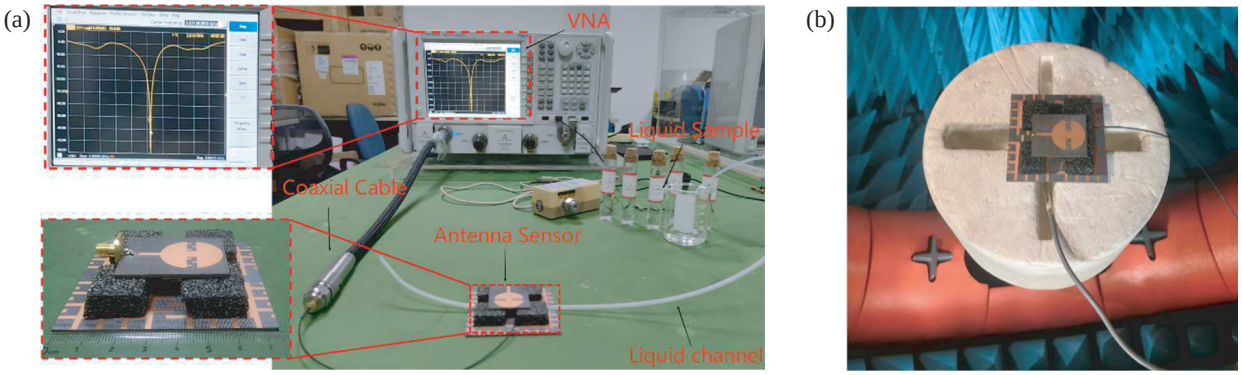

FIGURE 16. Photographs of the experimental setup. (a) The measurement environment. (b) The radiation pattern testing.

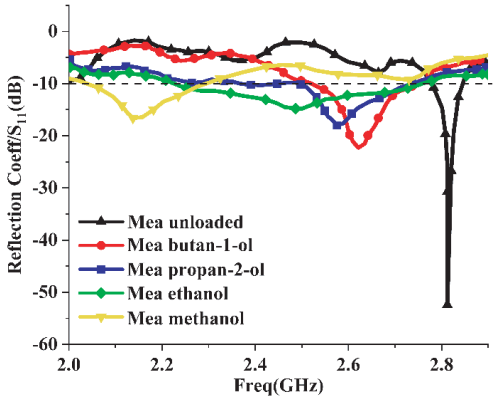

FIGURE 17. Measured results of the proposed sensor for various LUTs.

TABLE 2. Measured complex permittivity Parameters of different liquids.

LUT	Permittivity (ε_r)		RMS error	Loss tangent ($\tan\delta$)		RMS error
	This work	Reference	(%)	This work	Reference	(%)
Butan-1-ol	3.38	3.55	4.79	0.451	0.481	6.23
Propan-2-ol	4.04	3.8	5.94	0.613	0.642	4.52
Ethanol	5.83	6.18	5.66	0.882	0.96	8.13
Methanol	19.05	19.6	2.81	0.712	0.652	8.43

TABLE 3. Comparison of the proposed antenna and references.

Reference	Freq (GHz)	Sensitivity (%)	Relative size (λ_g^2)	Cover range (ε_r)	Non-contact
[21]	2.45	1.749	$1.18\lambda_g \times 1.18\lambda_g$	1–15	No
[25]	4.6	1.819	$3.25\lambda_g \times 3.25\lambda_g$	1–20	No
[26]	1.34	9.328	$1.19\lambda_g \times 2.01\lambda_g$	1–5	No
[27]	6.9	0.549	$3.49\lambda_g \times 3.49\lambda_g$	1–15	Yes
Proposed	2.8	2.342	$1.13\lambda_g \times 1.13\lambda_g$	1–25	Yes

ity for different LUTs had good linearity, and the goodness of fit reached 99.84%. In order to simulate the dielectric characteristics of the real liquid, the S_{11} response curve of the ideal liquid with $\varepsilon_r = 2$ is simulated after adding different loss tangent, as shown in Figure 13, and the resonant frequency is not sensitive to the change of loss tangent, but the trap depth and bandwidth show a certain trend change. According to Equation (5) that can be used to fit a linear curve with the inverse quality factor (Q^{-1}) of the sensor in different cases with the loss tangent, the curve is shown in Figure 14, and the curve equation can also inverse performance of different LUTs' loss tangent.

Figure 15 reflects the interrelationship between the relative permittivity of LUT, the inverse quality factor, and the loss tangent, and any two of the three variables are known to invert the approximate solution of the corresponding third variable using Equation (9). In summary, the S_{11} curves of the liquids loaded with different types of unknown liquids samples are tested by a vector network analyzer (VNA), and the data averages of the resonant frequency points and the two points corresponding to the Q-factor are obtained by multiple measurements to obtain the complex permittivity of the unknown liquid samples. Since all the mathematical models are established from simulation, the following physical tests will be performed to verify the accuracy of the theory.

$$\varepsilon_r = 35.79 f_r^2 - 203.9 f_r + 291.8 \tag{8}$$

$$\begin{aligned}\tan\delta = {} & (63.89Q^{-1} - 18.44\varepsilon_r - 11.15Q^{-2} \\ & -13.3Q^{-1}\varepsilon_r + 7.465\varepsilon_r^2 + 54.21) \times 10^{-2}\end{aligned} \tag{9}$$

4. MEASUREMENT AND RESULT DISCUSSION

Based on the structure of Figure 7, a physical device of the antenna sensor is fabricated as shown in Figure 16(a) for test verification. The antenna is supported by a non-conductive polystyrene foam with a thickness of 9 mm and a relative permittivity of 1.5 to simulate the propagation of electromagnetic waves in the air medium.

The reflection coefficient of the top antenna is measured using an Agilent N5242A PNA-X vector network analyzer when it is loaded with four different liquids, and the antenna is connected to the VNA through an SMA connector and a 50 Ω coaxial feed line. Figure 16(a) shows the final built measurement environment.

The results of the sensor measured unloaded and loaded with four different liquids, ethanol, methanol, butan-1-ol and propan-2-ol, are shown in Figure 17. The measured unloaded resonant frequency of 2.82 GHz is basically consistent with the simulation. The unloaded Q-factor reaches 352, due to errors in welding and fabrication, actual substrate dielectric constant deviation and measurement, and there is a certain gap compared to the simulation results of Q-factor 460. The overall trend is within the expected range, and the resonant frequency gradually decreases as the relative permittivity of the liquid increases.

The test data were recorded, and the final test results were compared with the reference table of the nominal values of the relative permittivity of liquids in the literature [24]. As shown in Table 2, the maximum error rate of the test for the real part of the complex relative permittivity was less than 6%, and the maximum error for the imaginary part was less than 8.5%. The test values basically agreed with the nominal values, which verified the accuracy of the sensor. The proposed liquid sensor is characterized by a compact structure, wide detection range, and high sensitivity, and it is suitable for applications such as instant monitoring of the dielectric characteristics of liquids.

Finally, the performance parameters of the developed sensor were compared with previous designs. The resonant frequency, size, maximum frequency shift, and detection range are shown in Table 3. It can be seen that the design has some application advantages in having a small relative size while achieving a relatively wide relative permittivity measurement range and non-contact measurement for the LUT.

5. CONCLUSION

In this paper, an antenna sensor based on inter-digital capacitor shape EBG structure is proposed for the complex permittivity measurement of liquid. It is different from the sensor of traditional planar resonant cavity type. The main structure is split into two parts: a detection antenna and an EBG structure. So it can realize noninvasive measurement and high sensitivity of the sensor at the same time.

Since the LUT is placed above the EBG structure, and it is not in contact with the detection antenna, the sensor can be applied to the real-time measurement of the complex permittivity of corrosive liquids.

The loading of different LUTs changes the equivalent capacitance between the EBG element and the antenna, which causes a shift in the antenna resonance frequency. By measuring S_{11} of the detection antenna, the complex permittivity of the LUT can be derived from the amount of resonant frequency shift and the amount of change in the inverse Q-factor. Samples of Butan-1-ol, Propan-2-ol, Ethanol, and Methanol were used to validate

the sensing performance. The root-mean-square (RMS) error for the real part of the measured complex permittivity is less than 6%, and the RMS error for the loss tangent is less than 8.5%.

REFERENCES

[1] Karuppuswami, S., L. L. Matta, E. C. Alocilja, and P. Chahal, "A wireless RFID compatible sensor tag using gold nanoparticle markers for pathogen detection in the liquid food supply chain," *IEEE Sensors Letters*, Vol. 2, No. 2, 1–4, Jun. 2018.

[2] Nitika, , J. Kaur, and R. Khanna, "Novel monkey-wrench-shaped microstrip patch sensor for food evaluation and analysis," *Journal of the Science of Food and Agriculture*, Vol. 102, No. 4, 1443–1456, Mar. 2022.

[3] Sung, P.-F., Y.-L. Hsieh, K. Angonese, D. Dunn, R. J. King, R. Machbitz, A. Christianson, W. J. Chappell, L. S. Taylor, and M. T. Harris, "Complex dielectric properties of microcrystalline cellulose, anhydrous lactose, and α-lactose monohydrate powders using a microwave-based open-reflection resonator sensor," *Journal of Pharmaceutical Sciences*, Vol. 100, No. 7, 2920–2934, Jul. 2011.

[4] Kale, V., S. Rath, C. Chavan, T. Bhave, and S. N. Kale, "Functionalised biosensor for diagnostics of dengue NS1 antigen: An integrated approach towards device development," in *2022 IEEE 7th International Conference for Convergence in Technology (I2CT)*, 1–5, 2022.

[5] Wang, P.-J., Y.-H. Pang, S.-Y. Huang, J.-T. Fang, S.-Y. Chang, S.-R. Shih, T.-W. Huang, Y.-J. Chen, and C.-K. Sun, "Microwave resonant absorption of SARS-CoV-2 viruses," *Scientific Reports*, Vol. 12, No. 1, 12596, Jul. 2022.

[6] Rossignol, J., A. Harrabi, D. Stuerga, P. Pribetich, G. Bailly, and T. Leblois, "Critical influence of dielectric sensitive material and manufactured process in microwave gas-sensing: Application of ammonia detection with an interdigital sensor," *ACS Omega*, Vol. 5, No. 20, 11 507–11 514, May 2020.

[7] Chen, Y., C. Hua, and Z. Shen, "Circularly polarized UHF RFID tag antenna for wireless sensing of complex permittivity of liquids," *IEEE Sensors Journal*, Vol. 21, No. 23, 26 746–26 754, Dec. 2021.

[8] Loutchanwoot, P. and S. Harnsoongnoen, "Microwave microfluidic sensor for detection of high equol concentrations in aqueous solution," *IEEE Transactions on Biomedical Circuits and Systems*, Vol. 16, No. 2, 244–251, Apr. 2022.

[9] Santra, M. and K. U. Limaye, "Estimation of complex permittivity of arbitrary shape and size dielectric samples using cavity measurement technique at microwave frequencies," *IEEE Transactions on Microwave Theory and Techniques*, Vol. 53, No. 2, 718–722, 2005.

[10] Wang, Y.-R. and H.-G. Hao, "Design of a microstrip sensor based on a CSRR-derived structure for measuring the permittivity and permeability of materials," *Progress In Electromagnetics Research M*, Vol. 111, 235–246, 2022.

[11] Hegazy, A. M., M. Alizadeh, A. Samir, M. Basha, and S. Safavi-Naeini, "Remote material characterization with complex baseband FMCW radar sensors," *Progress In Electromagnetics Research*, Vol. 177, 107–126, 2023.

[12] Fenner, R. A. and M. Shah, "A comprehensive error analysis of free-space techniques for extracting the permeability and permittivity of materials using reflection-only measurements," *Progress In Electromagnetics Research M*, Vol. 103, 151–159, 2021.

[13] Sagar, P. R. and P. N. Patel, "Metamaterial integrated rectangular waveguide with EM-wave localization for dielectric & moisture estimation of soil," *IEEE Sensors Journal*, Vol. 21, No. 20, 22 661–22 669, 2021.

[14] Riddle, B., J. Baker-Jarvis, and J. Krupka, "Complex permittivity measurements of common plastics over variable temperatures," *IEEE Transactions on Microwave Theory and Techniques*, Vol. 51, No. 3, 727–733, Mar. 2003.

[15] Alahnomi, R. A., Z. Zakaria, Z. M. Yussof, A. A. Althuwayb, A. Alhegazi, H. Alsariera, and N. A. Rahman, "Review of recent microwave planar resonator-based sensors: Techniques of complex permittivity extraction, applications, open challenges and future research directions," *Sensors*, Vol. 21, No. 7, 2267, 2021.

[16] Haq, T., C. Ruan, X. Zhang, S. Ullah, A. K. Fahad, and W. He, "Extremely sensitive microwave sensor for evaluation of dielectric characteristics of low-permittivity materials," *Sensors*, Vol. 20, No. 7, 1916, Apr. 2020.

[17] Alam, S., Z. Zakaria, I. Surjati, N. A. Shairi, M. Alaydrus, and T. Firmansyah, "Dual-band independent permittivity sensor using single-port with a pair of U-shaped structures for solid material detection," *IEEE Sensors Journal*, Vol. 22, No. 16, 16 111–16 119, Aug. 2022.

[18] Yeo, J. and J.-I. Lee, "High-sensitivity slot-loaded microstrip patch antenna for sensing microliter-volume liquid chemicals with high relative permittivity and high loss tangent," *Sensors*, Vol. 22, No. 24, 9748, 2022.

[19] Liu, C. and F. Tong, "An SIW resonator sensor for liquid permittivity measurements at C band," *IEEE Microwave and Wireless Components Letters*, Vol. 25, No. 11, 751–753, Nov. 2015.

[20] Seo, Y., M. U. Memon, and S. Lim, "Microfluidic eighth-mode substrate-integrated-waveguide antenna for compact ethanol chemical sensor application," *IEEE Transactions on Antennas and Propagation*, Vol. 64, No. 7, 3218–3222, Jul. 2016.

[21] Jun, S. Y., B. S. Izquierdo, and E. A. Parker, "Liquid sensor/detector using an EBG structure," *IEEE Transactions on Antennas and Propagation*, Vol. 67, No. 5, 3366–3373, May 2019.

[22] Arif, A., A. Zubair, K. Riaz, M. Q. Mehmood, and M. Zubair, "A novel cesaro fractal EBG-based sensing platform for dielectric characterization of liquids," *IEEE Transactions on Antennas and Propagation*, Vol. 69, No. 5, 2887–2895, May 2021.

[23] Yang, F. and Y. Rahmat-Samii, "Reflection phase characterizations of the EBG ground plane for low profile wire antenna applications," *IEEE Transactions on Antennas and Propagation*, Vol. 51, No. 10, 2691–2703, Oct. 2003.

[24] Gregory, A. P. and R. N. Clarke, "Tables of the complex permittivity of dielectric reference liquids at frequencies up to 5 GHz," *National Physical Laboratory Report*, 2012.

[25] Njogu, P. M., B. Sanz-Izquierdo, and E. A. Parker, "A liquid sensor based on frequency selective surfaces," *IEEE Transactions on Antennas and Propagation*, Vol. 71, No. 1, 631–638, Jan. 2023.

[26] Aquino, A., C. G. Juan, B. Potelon, and C. Quendo, "Dielectric permittivity sensor based on planar open-loop resonator," *IEEE Sensors Letters*, Vol. 5, No. 3, 1–4, 2021.

[27] Shi, Q., X.-W. Xuan, H.-K. Nie, Z.-Y. Wang, and W. Wang, "Antenna sensor based on AMC array for contactless detection of water and ethanol in oil," *IEEE Sensors Journal*, Vol. 21, No. 19, 21 503–21 510, 2021.